IEEE Access
Multidisciplinary | Rapid Review | Open Access Journal

Received March 9, 2022, accepted April 19, 2022, date of publication April 22, 2022, date of current version April 28, 2022.

Digital Object Identifier 10.1109/ACCESS.2022.3169787

Characterizing Scattering Parameters of Superconducting Quantum Integrated Circuits at Milli-Kelvin Temperatures

MANOJ STANLEY[1], (Member, IEEE), SEBASTIAN DE GRAAF[1], TERESA HÖNIGL-DECRINIS[2,3], TOBIAS LINDSTRÖM[1], AND NICK M. RIDLER[1], (Fellow, IEEE)

[1]National Physical Laboratory, Teddington TW11 0LW, U.K.
[2]Institute for Experimental Physics, University of Innsbruck, 6020 Innsbruck, Austria
[3]Institute for Quantum Optics and Quantum Information, Austrian Academy of Sciences, 6020 Innsbruck, Austria

Corresponding author: Manoj Stanley (manoj.stanley@npl.co.uk)

This work was supported in part by the U.K. Government's Department of Business, Energy and Industrial Strategy (BEIS) through the U.K. National Quantum Technologies Program; and in part by the U.K. Research and Innovation.

ABSTRACT Designing large-scale superconducting quantum circuits involves complex microwave engineering to minimize loss, spurious reflections, and signal crosstalk. Essential for engineering more complex circuits is precise knowledge of devices' microwave performance, which can be characterized by measuring its calibrated scattering parameters (S-parameters) at mK temperatures. In this work, we introduce a full 2-port calibrated S-parameter measurement setup which can characterize superconducting quantum integrated circuits and other RF integrated circuits operating at mK temperatures. The design and architecture of the measurement system consisting of in-house developed microwave calibration unit (MCU) housing the newly designed cryogenic calibration standards and the device under test (DUT) is discussed in detail. The measurement setup is then used to demonstrate the first calibrated S-parameter measurements of an in-house developed superconducting qubit integrated circuit at mK temperature.

INDEX TERMS Dilution refrigerator, low temperature measurements, microwave calibration, quantum integrated circuits, superconducting qubit circuit, vector network analyzer.

I. INTRODUCTION

Measurements of quantum integrated circuits at mK temperatures take on new importance today because of their immediate applications in quantum simulations [1], quantum sensing [2], and quantum computing [3]. One prominent technology for constructing a quantum computer involves superconducting qubits [4]. These are physically realised at the circuit level and implemented using nominally lossless capacitors, inductors, and Josephson junctions and packaged as integrated circuits [4]. Although these circuits operate only at mK temperatures inside a dilution refrigerator, all the additional supporting microwave components (directional couplers, circulators, isolators, amplifiers, attenuators, etc.) required to control and/or read out the quantum integrated circuits are often designed for use at higher temperatures (typically 10–300 K) and are merely assumed to operate normally at mK temperatures. However, when the entire setup including the microwave components is cooled to mK temperatures, the S-parameters of the components are likely to change. This makes it particularly challenging to design the whole microwave circuitry, as the successful operation of quantum circuits requires very good impedance matching and elimination of reflections [5].

In order to measure the actual S-parameters of a quantum integrated circuit at mK temperatures, a calibration scheme that shifts the reference planes of the measurement to the ends of the quantum circuit/device needs to be implemented, thus de-embedding the intervening passive and active components up to the ports of the vector network analyzer (VNA) measuring instrument, operating at room temperature.

Non-idealities in the measurement setup caused by imperfect connectors and cabling, and even the response of the test instrument will introduce errors into the measurements. For both transmission and reflection measurements, impedance mismatches within the test setup cause measurement uncertainties that appear as ripples superimposed on the measured data, when displayed in the frequency domain. These errors

The associate editor coordinating the review of this manuscript and approving it for publication was Chi-Yuan Chen.

can distort the signal and make it difficult to determine which reflections are from the DUT and which are from other sources. The calibration process effectively removes the systematic errors that cause uncertainty in measuring a DUT. During calibration, the VNA measures actual, well-defined standards and mathematically compares the results with ideal ''models'' of these standards. The accuracy of these calibration techniques depends on the availability of high-quality calibration standards. At low temperature, however, calibrating the set-up becomes more complicated since temperature will change the microwave characteristics of the calibration standards due to changes in physical characteristics of the materials such as their impedance, dielectric constant or physical size due to thermal contraction.

Previously, there have been demonstrations of one- and two-port calibrations for low temperature measurements, however, with several limitations. Some relied on using simulation results rather than actual measurements [6] and others relied on room temperature calibration for DUTs that operate at cryogenic temperatures [7]. In [8]–[10], the three standards were cooled down to low temperature through different thermal cycles before measuring the sample. The main drawbacks with these methods rely on the fact that the various cool-downs are not performed in perfectly identical conditions and that they do not fully consider the systematic errors induced by thermal gradients. Other techniques have been developed for measurements at 4K and higher temperatures [11]–[13] but were not directly suited for deployment at the mK stage. The most promising work in this area was demonstrated in [14], using a Thru-Reflect-Line (TRL) calibration method that was applied to connectorized coaxial DUTs operating at mK temperatures. Currently, there has been no demonstration of calibrated measurements of non-connectorized devices such as quantum integrated circuits operating at mK temperatures, and this capability is becoming more and more crucial for precision-engineering of large-scale quantum circuits. In this work, we have developed new cryogenic non-coaxial calibration standards to characterize non-coaxial components such as RF integrated circuits and quantum integrated circuits. Using our S-parameter measurement setup, we have demonstrated the calibrated S-parameters characterization of a superconducting qubit circuit at milli-kelvin temperatures for the first time.

Section II focusses on introducing an S-parameter measurement set up for characterizing quantum/RF integrated circuits at mK temperatures. The setup allows the circuits to be operated in the quantum regime without degrading their 'quantum performance', and to extract their RF characteristics. The microwave calibration unit (MCU) housing the custom developed cryogenic calibration standards and the DUT is explained in Section III. The calibration technique and the design of the calibration standards are also described in detail in Section III. Calibrated S-parameter measurements of a superconducting qubit circuit at mK temperatures is demonstrated in Section IV. The MCU deployed at mK temperatures has been designed to perform S-parameter measurements in the range 2-12 GHz, which is sufficient for most superconducting quantum computing applications.

II. CRYOGENIC S-PARAMETER MEASUREMENT SETUP

The architecture of the cryogenic S-parameter measurement setup which has been inspired and adapted from [14] to incorporate calibration standards to characterize non-connectorized devices is shown in Fig. 1. The dilution refrigerator is split into 6 stages of decreasing temperatures (∼300 K, ∼50 K, ∼4 K, ∼800 mK, ∼100 mK, and 20 mK) and consist of thermalized and attenuated RF lines and DC lines running through each of these stages.

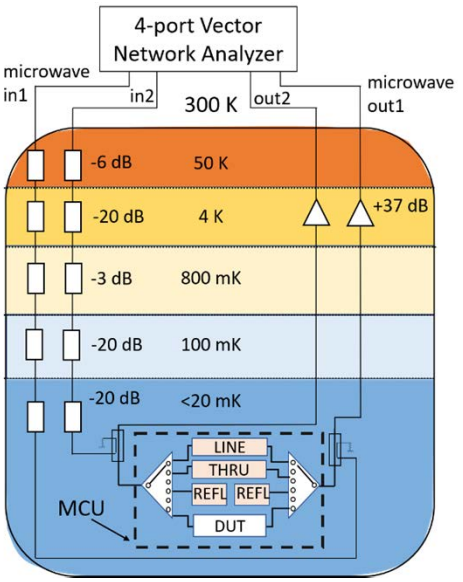

FIGURE 1. Cryogenic S-parameter measurement set-up.

The RF lines are realized as semi-rigid microwave cables and contain various microwave components such as attenuators, filters and amplifiers from the input side to the output side. While operating superconducting qubit circuits at mK temperatures, the number of thermal photons in the RF lines arriving at the coldest stage ($T < 20$ mK) of the dilution refrigerator should be well below the single photon level which can be achieved by adding a total attenuation of at least 60 dB in each of the RF input paths [15]. The bandwidth of the RF lines is chosen to be large enough to cover the typical frequency range of operation for superconducting quantum computing circuits (2-12 GHz). In the setup shown in Fig. 1, all four uncalibrated S-parameters are obtained by measuring the respective RF input and output coaxial lines which connects the MCU consisting of calibration standards and DUT at the coldest stage to the four ports of a commercial 4-port VNA such as Keysight Technologies PNA-X N5247B. The input RF signal is coupled to the MCU through cryogenic directional couplers with 20 dB directivity from 4 to 12 GHz. Wideband directional couplers operational from 0.3 to 18 GHz will be used for future measurements.

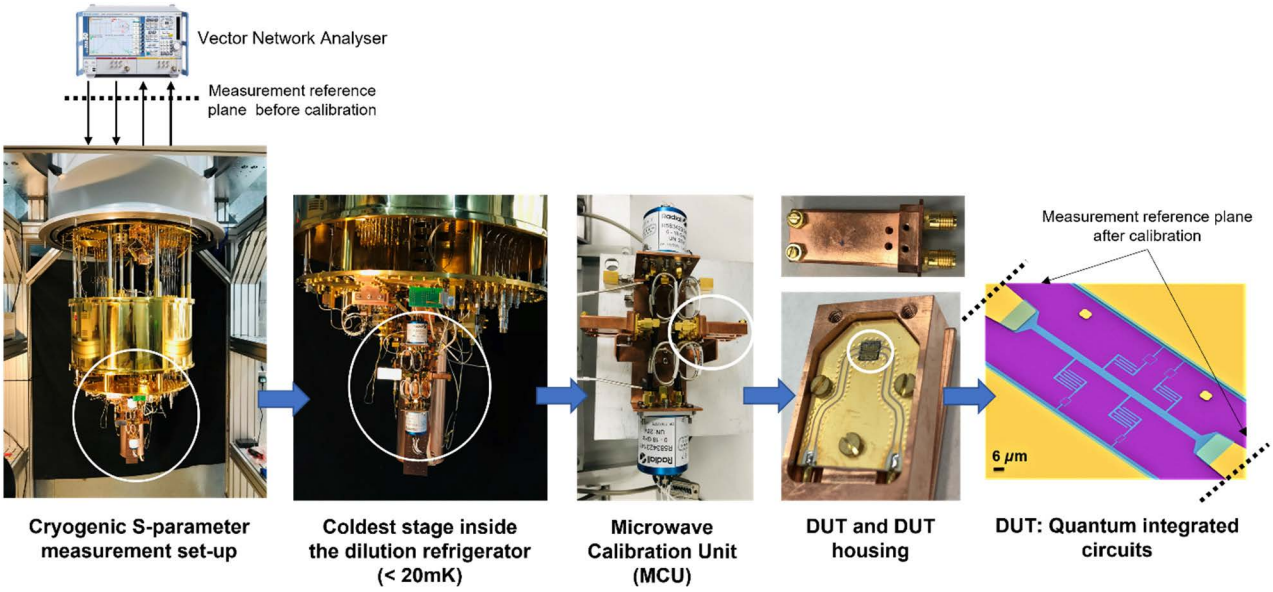

FIGURE 2. Calibrated S-parameter measurement set up to characterize quantum integrated devices at mK temperatures.

The RF power reaching the MCU for this setup is around −100 dBm which includes losses in cables, multi-stage attenuation and directivity of directional coupler. These are typical power levels at which quantum circuits operate and is required to limit the number of thermal photons in the RF lines arriving at the coldest stage (T < 20 mK) of the dilution refrigerator to be well below the single photon level [15]. It also ensures that any DUT or standard is not accidentally overheated by the calibration, which is likely to affect the result.

The output microwave signal from the MCU is amplified using a state-of-the-art high electron mobility transistor (HEMT) amplifier with ultra-low noise temperature of 2K anchored to the 4 K stage and having a gain of ∼37 dB and a frequency range of operation from 4 to 8 GHz (LNF-LNC4_8C). This amplifier is well suited for characterizing quantum integrated circuits due to their low noise performance [16], however, other models can be used to obtain a wider calibration frequency range on the expense of reduced noise performance. In this work we thus perform all the cold stage measurements in the frequency range 4-8 GHz, even though the calibration unit can work from 2-12 GHz.

The noise power is given by the amplifier input noise temperature ($T_0 = 2K$) and bandwidth (B) of 4 GHz of the first amplifier (HEMT LNA),

$$\begin{aligned} N_{dBm} &= 10\log_{10} kT_0B \\ &= 10\log_{10}(1.38 \times 10^{-23} \times 2 \times 4 \times 10^9) \\ &= -132\ \text{dBm} \end{aligned} \quad (1)$$

where k is the Boltzmann's constant.

As the RF power level (−100 dBm) is significantly larger than the noise power level (−132 dBm) in this case, there is minimal effect on the S-parameter measurements, when characterizing quantum circuits. The cryogenic amplifiers are followed by a 2-stage room temperature amplification which brings the signal levels as high as −20 dBm, which is sufficient input power for VNA measurements. If the RF power is reduced well below −100 dBm closer to the noise power level, dynamic range of measurements will be reduced, which will be evident when characterizing devices with very low reflection coefficient such as matched load or when characterizing the isolation level of an isolator. However, when characterizing such microwave components at mK temperatures, it is not strictly required to operate at such low RF power. The dynamic range and accuracy of measurements is further improved by employing noise reduction techniques such as operating the VNA at low IF receiver bandwidth (10 Hz) and using sweep averaging feature (averaging factor of 10) in the VNA.

Thorough thermalization of cables, attenuators, and microwave components at the various temperature stages of the dilution refrigerator is necessary for reducing the heat load on the dilution refrigerator and for protecting superconducting qubit circuits from thermal radiation and noise. In addition to thermal anchoring, filters with stop bands outside the frequency range of operation and infrared blocking Ecosorb filters further suppress thermal radiation.

Additional DC lines are used for biasing the cryogenic amplifiers, controlling RF switches and flux control of tuneable frequency qubits. These lines are made from twisted pair wires, typically low pass filtered and thermalized at each temperature stage [17].

III. MICROWAVE CALIBRATION

A. MICROWAVE CALIBRATION UNIT

Modern dry dilution refrigerators, which utilize pulse-tube cooling in place of liquid cryogens, have ample room at the mK stages. Therefore, it is possible to place relatively large microwave units at these mK temperatures. This in turn enables the application of improved and advanced calibration techniques as multiple calibration standards can be deployed inside the coldest stage of the refrigerator and microwave switches can be used to select the standards in situ thus saving calibration time. One full thermal cycle of the cryostat typically takes about 3 days, so a multiple-thermal-cycle calibration requiring 3 standards would require an additional 9 days for calibration. However, with RF switches built into the cryogenic MCU, all the calibration standards and DUT can be measured within the same thermal cycle in less than 2 hours. This also significantly reduces the drift and random errors in measurements and improves the quality of the calibration.

The MCU housing the RF switches, cryogenic calibration standards and the DUT is deployed in the coldest mK temperature stage in the dilution refrigerator as shown in Fig. 2, which also shows a zoomed image of the MCU and the DUT housing. The two RF switches (DC to 18 GHz) used in the MCU are commercially available mechanical pulse latched Radiall SP6T switches that operate by means of electrical pulses (5 Vpp) of short duration (10 ms) to latch the switch to different positions, so no electrical signal is applied to the switch in its quiescent state. These are software controlled to activate/deactivate the respective standard/DUT during the measurements. A switching pulse only results in a very moderate increase in cryostat temperature of a few 10's of mK, which is important because the quantum circuits must not be overheated.

The calibration technique is applied to shift the calibration reference planes from the VNA test ports to the ends of the DUT. In this work, we demonstrate the characterization of S-parameters of a quantum integrated circuit consisting of multiple superconducting qubits as the DUT. The DUT was designed to function as an absolute-power quantum sensor at mK temperatures, described in detail in [18].

B. CALIBRATION STANDARDS AND ALGORITHM

The Thru-Reflect-Line (TRL) technique can be used to calibrate non-connectorized devices fabricated in non-coaxial medium such as microstrip, coplanar waveguide (CPW), etc [19]. The advantages of the TRL calibration are (i) the use of redundant calibration standards reduces the uncertainty due to errors, such as connector repeatability, cable flexure, test-set drift, and noise, and (ii) the foundation of the calibration standard definitions depend solely on qualitative requirements (uniformity of the lines, identical cross-sections of the lines, and identical reflection coefficients of the Reflect standards) without having the need to precisely characterize the standards, compared to calibration techniques such as Short-Open-Load-Thru, making it more suitable for use at mK temperatures. It is also difficult to design a precise Load standard operating at mK temperatures.

The TRL calibration corrects systematic errors caused by imperfections in the VNA and test setup based on an 8-term error model [20]. The systematic errors are repeatable and assumed to be time invariant and can be characterized during the calibration process and mathematically removed during measurements unlike the drift and random errors. The TRL calibration accounts for systematic errors such as directivity, source match and reflection tracking which are generated due to reflections in the measurement setup. It can also correct load match errors and transmission tracking errors, which are generated due to transmission measurements [20].

The Thru, Reflect and Line standards are designed, and fabricated, using separate PCBs as grounded co-planar waveguide (GCPW) transmission line structures as shown in Fig. 3(a). A GCPW structure is chosen as it provides better thermalisation of the PCB and DUT at mK temperatures. In addition, there is an additional advantage of reduction in crosstalk between the two ports as the ground trace surrounding the central conductor is grounded through vias. Rogers RO4350B with relative permittivity 3.48 and loss tangent 0.0037 at 10 GHz at room temperature is used as the PCB substrate. The size of each of the PCB boards is 20.4 mm $\times$ 14.7 mm with a thickness of 0.5 mm. The top and bottom copper ground planes of 1.4 mil ($\approx$36 μm) thickness are connected by using shorting filled via holes of 0.5 mm diameter. The design dimensions of the GCPW structure (such as the center conductor width, the gap width between the center conductor and the two grounds, and substrate thickness) are estimated by solving the analytical equations in [21] for a characteristic impedance of GCPW transmission line of 50 Ω and optimized using CST Microwave Studio simulations.

The middle of the Thru PCB standard is set as the reference plane. The Reflect standard could be realized as a pair of short-circuits or open-circuits, with two nominally identical short/open-circuits implemented on a single PCB to provide the two Reflect standards. The reflection coefficient of both these short/open-circuit standards does not need to be known at mK temperatures; however, they should be identical for a good quality calibration [21]. The Line standard is implemented as an extra section of transmission line that provides a change in the transmission phase, with respect to the Thru connection. In a $^1/_4$-wave TRL calibration, the Line standard is designed to provide a change in the transmission phase, with respect to the Thru connection, of approximately 90° – i.e. $^1/_4$-wavelength– at frequencies around the middle of the frequency band. The calibration failure points occur at 0° and 180°. Therefore, when implementing a $^1/_4$-wave TRL calibration procedure, phase changes are designed to be at least 20° greater than 0° and at least 20° less than 180°. In this work, a single line standard is designed to be 6 mm (i.e. $^1/_4$ of the GCPW wavelength at 7 GHz) longer than the Thru standard to cover the frequency range of 2-12 GHz.

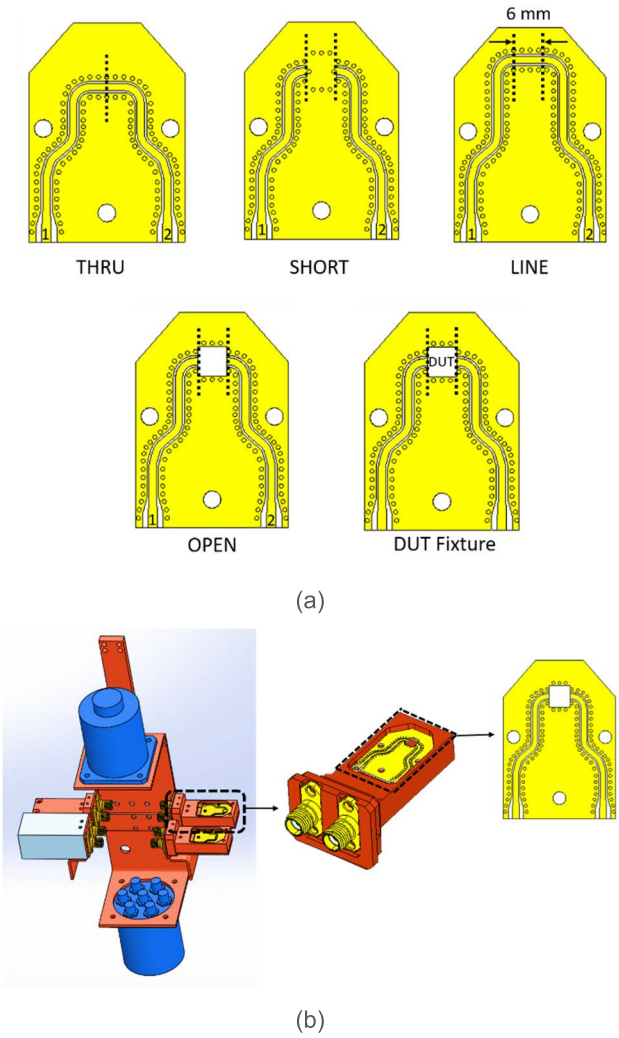

FIGURE 3. (a) PCBs containing the various Thru-Reflect-Line standards with reference planes and port numbers marked (b) The MCU layout including DUT and standards.

The DUT is connected to the transmission lines on both sides of the DUT fixture PCB, as shown in Fig. 3(a), either via solder or using wire bonds.

For characterization of quantum integrated circuits such as superconducting qubit circuits, the DUT along with the PCB fixture and each of the calibration standards are typically enclosed within a specialized metal box as shown in Fig. 3 (b). The sealed box is made from copper for good thermal anchoring and shielding of the device from thermal photons. The box shown here is specifically adapted for the superconducting quantum sensor discussed in [18], but can accept any integrated circuit of size up to ∼5 mm × 5 mm. The GCPW PCB for each standard and DUT is fabricated using the Electroless Palladium Autocatalytic Gold (EPAG) process with gold finish which is non-magnetic and suitable for wire bonding. A U-shape based calibration standard is used instead of a straight one to implement the standards within the metal box. The PCB standards are soldered inside these metal boxes which are fitted with SMA connectors. Coaxial-to-GCPW transitions are added to the ends of the PCB standards to ensure radiation free wave propagation, and hence minimize any degradation of the microwave calibration.

The suitability of the fabricated calibration standards for use with the TRL calibration technique is tested at room temperature by characterizing a commercial 10 dB microwave attenuator before deploying the standards in the dilution refrigerator. The PCB circuitry inside of a 10 dB coaxial attenuator [22] was used as the DUT by connecting it to the PCB fixture within the metal box using wire bonds. The measured S-parameters of the attenuator are shown in Fig. 4. The reflection coefficient performance is good (i.e. better than −10 dB) and agrees with the manufacturer's specification. Also, the variations in S_{21} from 10 dB are less than 0.6 dB up to 6 GHz, which again agrees with the manufacturer's specifications. The tested calibration standards and DUT are attached to a copper mounting plate as shown in Fig. 3(b) and connected to the ports on the RF switches via a set of short (76 mm) and nominally identical commercial semi-rigid SMA coaxial cables with aluminium jacket to the MCU, which then connects to the VNA through the rest of the dilution refrigerator hardware. The effect of wire bonds in the S-parameter results is currently being investigated and will be reported in a future publication.

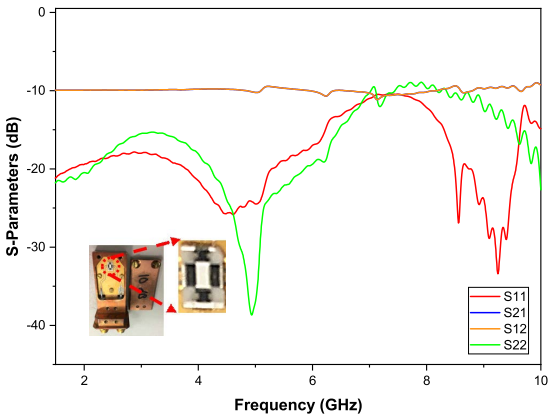

FIGURE 4. Measured S-parameters of a commercial 10 dB attenuator characterized using the TRL calibration kit at room temperature.

To extract the actual S-parameters of the DUT at mK temperatures, the uncalibrated S-parameters of the DUT and the TRL calibration standards are recorded, and then an offline TRL calibration routine is applied to solve the 8-term error model. The VNA switch correction terms have been measured to be negligible for this configuration due to the high attenuation in the forward position and due to the high isolation of the amplifiers in the reverse position and is hence not incorporated in the error model for TRL calibration. These terms are usually included in the 12-term error model to account for the change in reflection coefficient at the VNA's internal switch as it is switched from the forward to reverse positions [23]. The reference impedance of the calibration is

the characteristic impedance of the line standard. If necessary, the measured S-parameters can be renormalized to a desired impedance by estimating the characteristic impedance of the transmission line [24], [25].

C. CALIBRATION ERRORS

The part of the measurement setup from the room temperature VNA down to the low temperature RF switches is accounted for in the error model during calibration. The calibration algorithm assumes that the calibration standards and DUT fixtures are identical up to the calibration reference plane. The cryogenic RF switch ports and the cables connecting the RF switches to the standards and devices need to be as identical as possible at mK temperatures to minimize calibration errors.

The RF switch ports can create differences in transmission paths and return losses intrinsic to the switches. The variation in the performance of RF switch ports is investigated by characterizing one of the RF switches at room temperature. The calibrated S_{21} with measurement reference planes at the common input port of the switch and each activated output port is measured and plotted in Fig. 5(a). The maximum variation in the transmission coefficient between the various transmission paths is within 0.006 dB in the given frequency range.

The variation in S_{21} is linear scale defined as

$$\varepsilon_{21}^{max} = max_{i,j=1\ldots6}\left(\left|S_{21}^{i} - S_{21}^{j}\right|\right) \tag{2}$$

The variation in S_{11} is defined as

$$\varepsilon_{11}^{max} = max_{i,j=1\ldots6}\left(\left|S_{11}^{i} - S_{11}^{j}\right|\right) \tag{3}$$

The reflection coefficients of all the RF output switch ports were measured and found to be less than -27 dB as shown in Fig. 5(b) and so any variation in reflection coefficient between these ports are considered small enough to be neglected.

The switch repeatability errors of the RF switch port is measured by switching ON and OFF one of the RF switch output ports multiple times and measuring the transmission coefficient between this output port and the common input port of the switch in the ON state. The results in Fig. 6 shows that the variation in transmission coefficient is within 0.005 dB. The impact of the switch port variations on the calibration depends on the affected path (DUT or standards). The worst case is when only the DUT path is affected because the errors affect the calibration coefficients directly. The worst-case effect of the switch port differences on the DUT S-parameters is given by [36],

$$\Delta S_{11}^{DUT} = S_{11}^{DUT} \pm \varepsilon_{11}^{max,var1} \tag{4}$$

$$\Delta S_{21}^{DUT} = S_{21}^{DUT}(1 \pm \varepsilon_{21}^{max,var1} \pm \varepsilon_{21}^{max,var2} \pm \varepsilon_{21}^{max,rep1} \pm \varepsilon_{21}^{max,rep2}) \tag{5}$$

where $\varepsilon_{21}^{max,var1}$ and $\varepsilon_{21}^{max,var2}$ are the transmission loss errors due to variation in switch ports in RF switch 1 and RF switch 2 respectively and $\varepsilon_{21}^{max,rep1}$ and $\varepsilon_{21}^{max,rep2}$ are the transmission loss errors due to repeatability of switch ports in RF switch 1 and RF switch 2 respectively. The maximum variation in reflection performance due to variation in switch ports in RF switch 1 is denoted by $\varepsilon_{11}^{max,var1}$.

The variations in the microwave path connecting the low temperature RF switches and the devices (cables, connectors, device fixtures) can also create calibration errors. Connector repeatability errors will be introduced due to the differences in the return loss performance of the SMA connectors used with the metal box standards, variations in soldering of the SMA connector to the PCB standards/DUT, RF switch ports and cables. These can generally be controlled by using good quality RF components. The cable performance is investigated by characterizing the transmission coefficient at room temperature as shown in Fig. 7. In the given frequency range, the maximum variation between the six nominally identical RF SMA cables was within 0.006 dB.

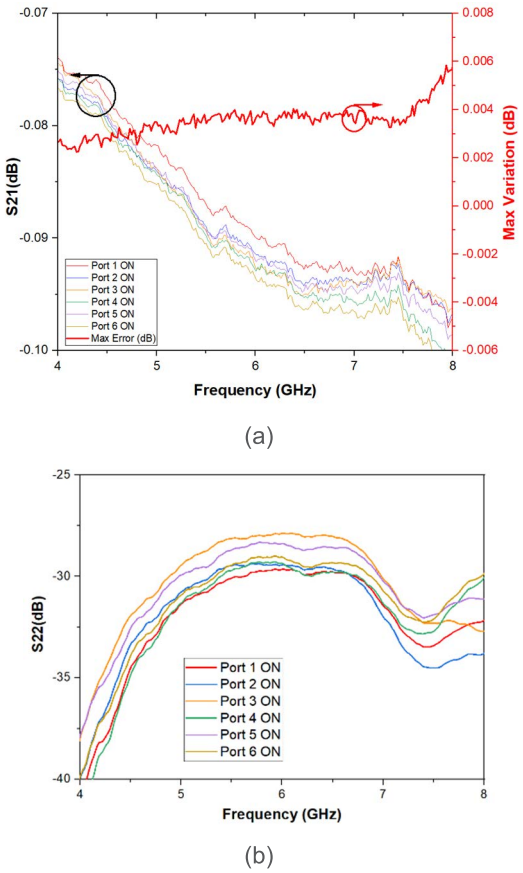

FIGURE 5. Measured variability in performance of SP6T RF switch ports at room temperature (a) Transmission coefficient (S_{21}); (b) Reflection coefficient (S_{22}).

An important caveat for the measurement of the switch and test-cable symmetry is the fact that these measurements are performed at room temperature and not at the cryogenic temperatures at which the DUT and standards are measured. To precisely estimate the variability and repeatability of the RF switch ports and the variability of

cables at mK temperatures, the RF switches along with the cables will need to be characterized in detail as a DUT at mK temperatures. As the RF switches are coaxial devices, an S-parameter measurement setup employing coaxial calibration standards will need to be designed and setup to measure the calibrated S-parameters of RF switches. This is planned as a future activity and is beyond the scope of this work. At low temperatures, the cables must be connected in a symmetric configuration to have identical temperature effects on each cable such as differential thermal contraction at mK temperatures. The impact of the cable variations on the calibration depends on the affected path (DUT or standards).

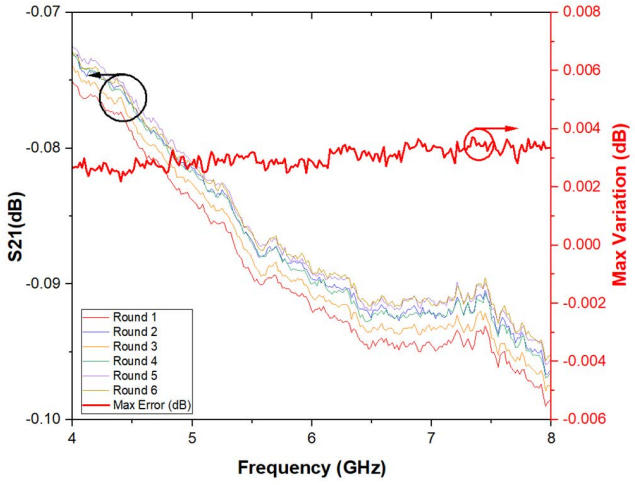

FIGURE 6. Measured repeatability in transmission coefficient when Port 1 of one of the SP6T RF switches is repeatedly turned ON at room temperature.

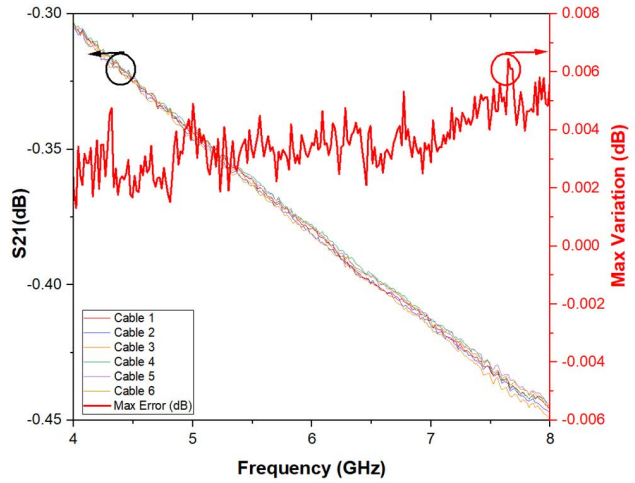

FIGURE 7. Measured variability in performance of transmission coefficient for 6 nominally identical short (15 cm) commercial male to male RF SMA cables attached to one of the RF switches at room temperature.

During the extended period of the measurement cycle, any drift occurring due to temperature changes inside and outside the dilution fridge will introduce drift errors in calibration. Cable movements in the room temperature stage can also introduce drift errors. The variations at room temperature can create drifts in the amplifier stage, cables, and the VNA. By regularly re-calibrating the measurement system, drift errors can be minimised. To demonstrate the performance variation due to temperature variations at mK, the maximum variation in the uncalibrated forward transmission coefficient of the Thru standard observed for a range of different temperatures (15-40mK) and several switching cycles is plotted in figure 8, determined using eq (5). The variation in S_{21} can be as much as 0.18 dB which would create significant error in subsequent measurements. Hence, it is necessary to minimise any change in temperature while operating the RF switches at the mK stage.

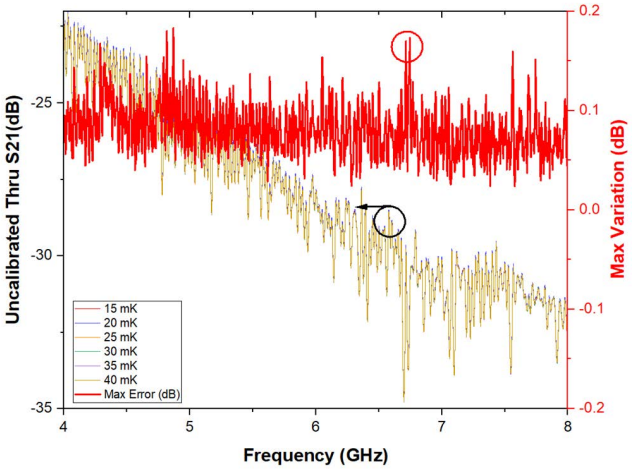

FIGURE 8. Variation in transmission coefficient performance due to temperature changes and switching in the mK stage.

IV. DEVICE CHARACTERIZATION

Using the cryogenic MCU, quantum integrated circuits such as superconducting qubit circuits or other passive or active RF integrated circuits (RFICs), such as attenuators, power amplifiers, isolators, etc., can be characterized by reliable measurements. In this section, the calibrated S-parameters of an in-house developed superconducting flux qubit embedded in an IC [17] as the DUT is characterized at mK temperatures. The DUT is wire bonded to the GCPW PCB which is enclosed within the copper box and a shield made of superconducting aluminium to reduce magnetic noise. The device was designed to function as an absolute power quantum sensor at mK temperatures and can be inserted as an additional low loss element into the transmission line close to the reference plane of another device to facilitate calibration of transmission lines, microwave components or devices within dilution refrigerators. The detailed operating principle of the quantum-based sensor is described in [17] and [26].

This specific DUT consisted of five independent flux qubits in the same IC, positioned in the gap between the signal and ground lines of the through CPW transmission-line on the IC. The flux qubits are lithographically defined

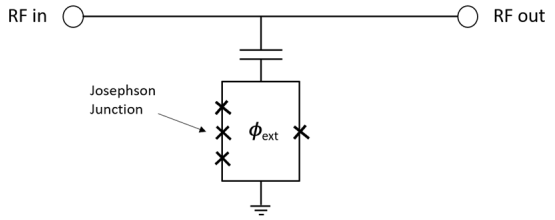

FIGURE 9. Simplified circuit diagram of a single flux qubit which acts as a non-linear shunt admittance across the transmission line when tuned into resonance.

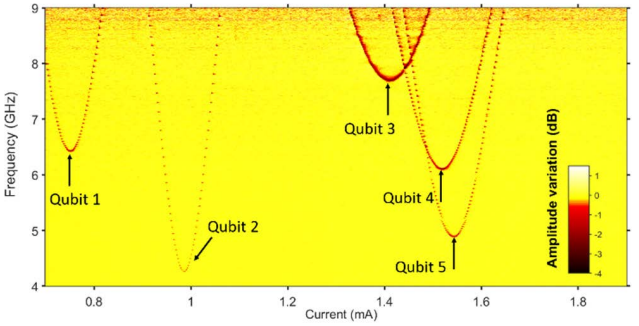

FIGURE 10. Normalized forward transmission, S21 amplitude spectrum of five flux qubits as a function of incident microwave frequency and current through an external superconducting coil providing the flux bias that tunes the qubit frequency.

micrometer sized loops of superconducting metal interrupted by Josephson junctions. Each flux qubit is frequency tuneable by application of a small magnetic field B resulting in a magnetic flux Φ_{ext} threading the superconducting loop of area A. The frequency difference between ground and excited state of the flux qubit changes approximately as

$$f = h\sqrt{(2E_L(\Phi_{ext}/\Phi_0 - 1/2))^2 + \Delta^2} \quad (6)$$

$$\Phi_{ext} = B \times A \quad (7)$$

where $\Phi_0 = 2.068 \times 10^{-15}$ Wb is the magnetic flux quantum, E_L the inductive energy of the loop and Δ is the minimum energy of the qubit determined by the Josephson junction properties. The external magnetic field, B, is changed by applying a current, I, through an external superconducting coil placed in the MCU enclosure for the DUT as shown in Fig. 3(a). The application of a magnetic field results in approximately a parabolic frequency dependence described by eq. (6) with a minimum frequency at $\frac{\Phi_{ext}}{\Phi_0} = 1/2$. The simplified circuit diagram of a single flux qubit used in the sensor IC is shown in Fig. 9. Five of these flux qubits are present in series along the IC CPW transmission line and can be accessed independently. Their behaviour can be described as a narrow-band and frequency tuneable shunt admittance at low RF power, resulting in additional reflection and absorption of incoming microwave signal. At high RF power the qubit is saturated and does not scatter the microwave signal, which is another reason why calibration of quantum ICs needs to be performed with large input line attenuation and at very low signal levels.

To detect each flux qubit, the frequency of the incident microwave signal is swept over a wide range using the VNA, monitoring the transmission (S_{21}, in this case) response of the sensor IC at various currents, I. The amplitude of S_{21} at each frequency and each current, I, is measured and normalized against the amplitude of S_{21} at zero current and plotted in Fig. 10. The resonant frequency of each flux qubit can be observed to be varying as a parabolic function between current and frequency in accordance with eq. (6), and the qubit properties and coherence is similar to when measured separately (without the calibration setup). The measured response of each qubit strongly depends on frequency, intrinsic qubit properties, its coupling to the transmission line, and the driving power, which results in qubits appearing with different intensity and widths as seen in Fig 10. The normalized transmission graphs provide information about the relative change in transmission coefficient due to the qubits, however, to understand the absolute transmission, reflection or the insertion loss of the DUT IC, a full S-parameter calibration is required.

As a first step, the calibrated S-parameters of the sensor are investigated when all the qubits are tuned outside the relevant frequency band (here corresponding to zero current supplied by the external solenoid). In this configuration, there will be no coupling of RF power from the transmission line to the qubits. The raw S-parameters data of the standards and the DUT is recorded and then the calibration algorithm is applied to obtain the calibrated S-parameters of the DUT. The calibrated response of the DUT in Fig. 11(b) shows significant improvement in the visualization of the device behaviour, when compared with the uncalibrated DUT data in Fig. 11(a), by removing the unwanted electrical effects caused by the presence of cables and other microwave components. It can be seen from Fig. 11(b) that the reflection coefficients at both ports are very similar and less than -10dB indicating a good impedance match at both ports with respect to the transmission line impedance. The transmission coefficient in Fig. 11(b) shows that the insertion loss is below 1 dB from 4-8 GHz which agrees with the findings in [17] that the DUT is low loss and does not affect significantly the performance of an external circuitry if inserted as an additional element for calibrating transmission lines or devices at mK temperatures.

Now, we investigate the calibrated S-parameters when one of the qubits shown in Fig. 10 is tuned into the frequency band by applying a small current to the external solenoid ($I = 0.751$ mA). Fig. 12(a) shows the uncalibrated response. Here it is very difficult to extract anything meaningful from the raw data. However, in the TRL calibrated response in Fig. 12(b), the qubit resonant frequency can be easily observed in the transmission coefficient response (S_{21} and S_{12}) at 6.5 GHz. The reflection coefficient response (S_{11} and S_{22}) at both ports are very similar and agree well with the reflection coefficient curves shown in Fig. 11(b), except near the resonant frequency. This also confirms that the only change in energy reflected from the sensor ports from

qubit decoupled state to "qubit 1" coupled state is due to the qubit coupling at a narrow band around the qubit resonant frequency. By exciting each of the five qubits separately with the respective current, I and plotting their corresponding calibrated S-parameters, no change in transmission or reflection coefficient can be observed except at the narrow band around the respective qubit resonant frequency. This is a very useful insight as it demonstrates through S-parameter measurements that there are no other unwanted non-uniform mode coupling behavior occurring within the sensor when any of their qubits are excited, which will compromise its use as a power sensor. It is also useful to see that the insertion loss for the sensor at different current drive remains the same, except at the respective qubit resonant frequencies.

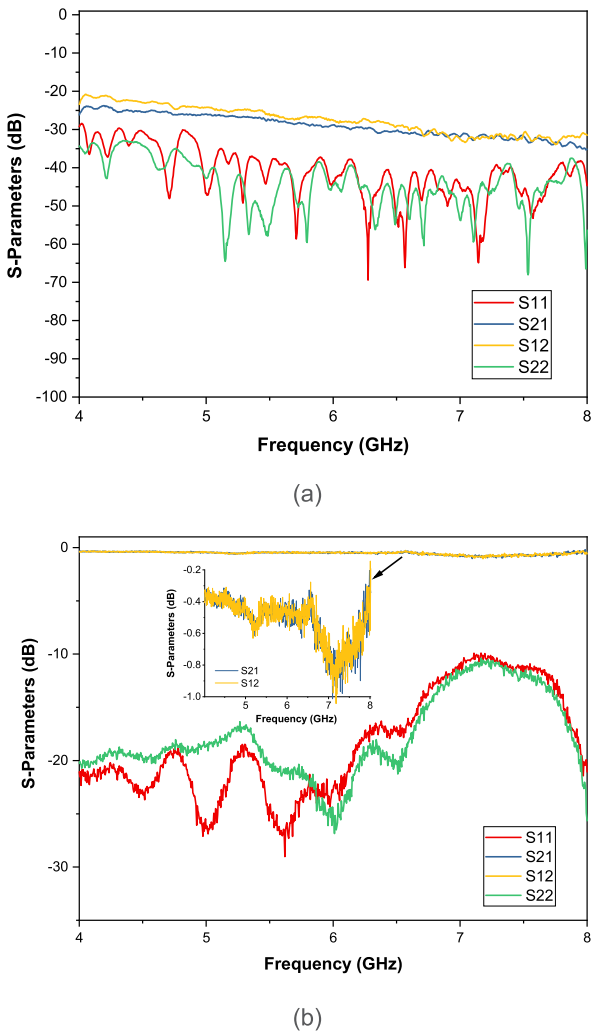

FIGURE 11. S-parameters of the superconducting qubit circuit at 0 mA current drive (a) before calibration; (b) after calibration. The inset shows a close-up of the transmission parameters.

In Fig. 13, the TRL calibrated forward transmission coefficient for qubit 1 is compared with two different normalization approaches. As explained in Section III. B, the TRL algorithm can correct reflection and transmission systematic errors such as directivity, source match and load match, reflection and transmission tracking. A full 2-port TRL calibration is necessary to extract the calibrated forward and reverse transmission coefficients and reflection coefficient of both ports.

The Thru response calibration is an approximate normalization approach requiring only a Thru standard which corrects only for the frequency response errors. This is represented by:

$$S_{21,norm}\,(dB) = S_{21,uncal}\,(dB) - Sthru_{21,unccal}\,(dB) \quad (8)$$

where $S_{21,norm}$ is the Thru response normalized S_{21} of the DUT, $S_{21,uncal}$ is the uncalibrated S_{21} of the DUT and $Sthru_{21,unccal}$ is the uncalibrated S_{21} of Thru standard. This technique results in residual errors which can clearly be seen as ripples in the normalized S_{21} data in Fig. 14, thus giving a poor estimate of insertion loss across the frequency range.

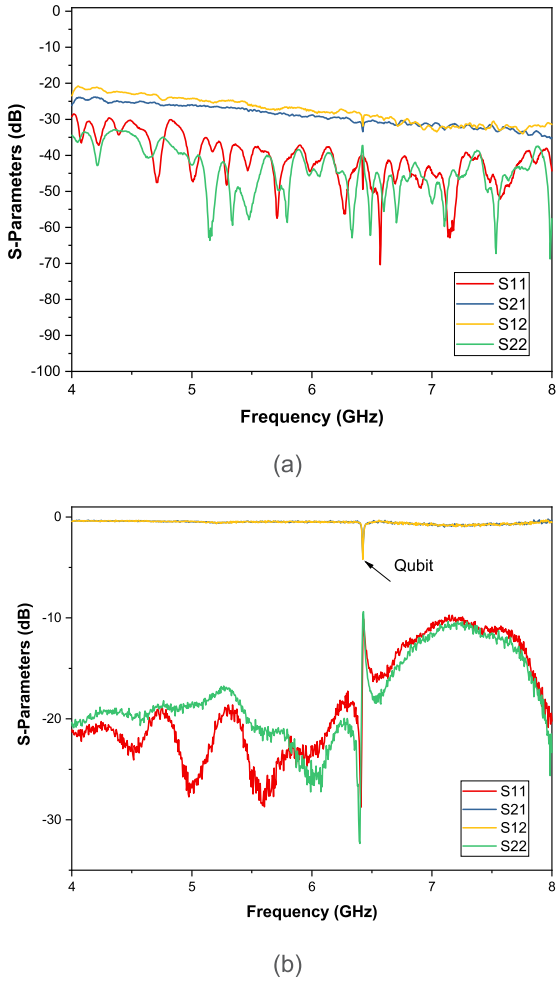

FIGURE 12. S-parameters of the superconducting qubit circuit when "qubit 1" is tuned by applying a small current to the external solenoid (I=0.751 mA) (a) before calibration; (b) after calibration.

Another normalization approach commonly used is to normalize the transmission coefficient of the sensor for a particular current drive with respect to the transmission coefficient

at zero current drive. This is represented by:

$$S_{21,norm}\,(dB) = S_{21,\ I=I0}\,(dB) - S_{21,\ I=0mA}\,(dB) \qquad (9)$$

where $S_{21,norm}$ is the normalized S_{21} of the sensor, $S_{21,I=I0}$ is the uncalibrated S_{21} of sensor at current drive, $I = I0$ and $S_{21,I=0\ mA}$ is the uncalibrated S_{21} of sensor at $I = 0\ mA$.

Although the normalization method (normalized to zero current drive) helps to visualize the changes due to the qubit circuit such as its resonance frequency through the forward transmission coefficient, the disadvantage with the technique is that other sensor specific information such as insertion loss is lost. It is also not possible to extract the return loss/calibrated reflection coefficient and reverse transmission coefficient of the DUT ports through the normalization method. For example, in theory, the ideal qubit should be on resonance in the low power limit resulting in complete destructive interference in the forward direction of transmission and complete constructive interference in the backward propagating direction [27], i.e. neglecting on-chip losses we expect to observe $S_{11} = 0$ dB and $S_{22} = 0$ dB on resonance. From Fig. 12b we can see that this is clearly not the case, on resonance each qubit still has a significant return loss. This can be due to power saturation, qubit imperfections and/or due to reflections elsewhere on the IC, which could be disentangled in more detailed experiments using this calibration setup.

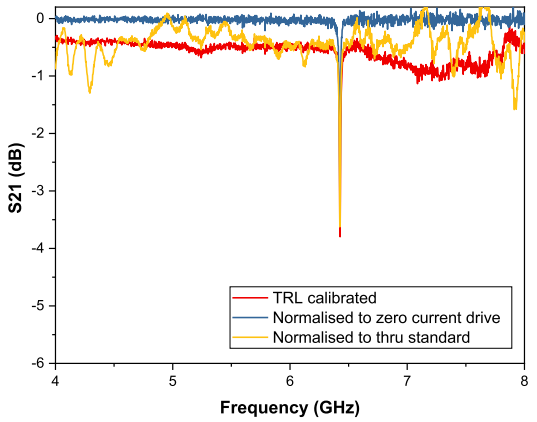

FIGURE 13. Calibrated forward transmission coefficient (S_{21}) of "qubit 1" using several techniques described in the text.

The full two-port calibrated S-parameters of quantum IC's also enables the precise identification of issues including insertion loss, spurious reflections and crosstalk in quantum circuits across a broad parameter range that might limit device performance. This will be of great value in validating RF performance and material properties in increasingly complex quantum circuits such as quantum processors [27], cryogenic classical ICs that control quantum circuits [28], and on-chip microwave components such as signal generators [29], Josephson circulators [30], [31], switches [32], tunable couplers [33], or quantum limited amplifiers [34], or other types of quantum microwave photonic devices [35].

V. CONCLUSION

In this work, the authors have presented the design of a full 2-port S-parameter measurement setup capable of performing calibrated measurements of superconducting quantum integrated circuits and RF integrated circuits at mK temperatures. An MCU, consisting of newly developed cryogenic calibration standards has been designed and deployed at the mK stage inside a dilution refrigerator. The measurement setup can perform calibrated S-parameter measurements in the range of up to 2-12 GHz which is sufficient for most quantum computing applications. The setup was then used to demonstrate the calibrated S-parameter measurements of a superconducting qubit circuit at mK temperatures. The "true" device performance is obtained from the calibrated measurements which showed improvement in the visualisation of the qubits by removing the unwanted effects of cables and other microwave components. This measurement capability will accelerate design and development of new and improved quantum and microwave devices operating at mK temperatures to advance quantum computing research.

ACKNOWLEDGMENT

Quantum ICs were fabricated in the SuperFab cleanroom at Royal Holloway, University of London.

REFERENCES

[1] I. M. Georgescu, S. Ashhab, and F. Nori, "Quantum simulation," *Rev. Modern Phys.*, vol. 86, p. 153, Mar. 2014.

[2] C. L. Degen, F. Reinhard, and P. Cappellaro, "Quantum Sensing," *Rev. Modern Phys.*, vol. 89, no. 3, Jul. 2017, Art. no. 035002.

[3] M. Kjaergaard, M. E. Schwartz, J. Braumüller, P. Krantz, J. I.-J. Wang, S. Gustavsson, and W. D. Oliver, "Superconducting qubits: Current state of play," *Annu. Rev. Condens. Matter Phys.*, vol. 11, no. 1, pp. 369–395, Mar. 2020.

[4] P. Krantz, M. Kjaergaard, F. Yan, T. P. Orlando, S. Gustavsson, and W. D. Oliver, "A quantum engineer's guide to superconducting qubits," *Appl. Phys. Rev.*, vol. 6, no. 2, Jun. 2019, Art. no. 021318.

[5] M. Jerger, A. Kulikov, Z. Vasselin, and A. Fedorov, "*In situ* characterization of qubit control lines: A qubit as a vector network analyzer," *Phys. Rev. Lett.*, vol. 123, no. 15, Oct. 2019.

[6] M. S. Jun, S. W. Hwang, D. Y. Jeong, and D. Ahn, "Microwave design and characterization of a cryogenic dip probe for time-domain measurements of nanodevices," *Rev. Sci. Instrum.*, vol. 75, no. 7, pp. 2455–2460, Jul. 2004.

[7] J. C. Booth, D. H. Wu, and S. M. Anlage, "A broadband method for the measurement of the surface impedance of thin films at microwave frequencies," *Rev. Sci. Instrum.*, vol. 65, no. 6, pp. 2082–2090, Jun. 1994.

[8] H. Kitano, T. Ohashi, and A. Maeda, "Broadband method for precise microwave spectroscopy of superconducting thin films near the critical temperature," *Rev. Sci. Instrum.*, vol. 79, no. 7, Jul. 2008, Art. no. 074701.

[9] M. L. Stutzman, M. Lee, and R. F. Bradley, "Broadband calibration of long lossy microwave transmission lines at cryogenic temperatures using nichrome films," *Rev. Sci. Instrum.*, vol. 71, no. 12, p. 4596, 2000.

[10] K. Steinberg, M. Scheffler, and M. Dressel, "Broadband microwave spectroscopy in Corbino geometry at 3He temperatures," *Rev. Sci. Instrum.*, vol. 83, no. 2, Feb. 2012, Art. no. 024704.

[11] D. E. Oates, R. L. Slattery, and D. J. Hover, "Cryogenic test fixture for two-port calibration at 4.2 k and above," in *Proc. 89th ARFTG Microw. Meas. Conf. (ARFTG)*, Jun. 2017, pp. 1–4.

[12] J.-H. Yeh and S. M. Anlage, "*In situ* broadband cryogenic calibration for two-port superconducting microwave resonators," *Rev. Sci. Instrum.*, vol. 84, no. 3, Mar. 2013, Art. no. 034706.

[13] P. Diener, F. Couëdo, C. Marrache-Kikuchi, M. Aprili, and J. Gabelli, "Cryogenic calibration setup for broadband complex impedance measurements," in *Proc. AIP Conf.*, 2014, pp. 113–118.

[14] L. Ranzani, L. Spietz, Z. Popovic, and J. Aumentado, "Two-port microwave calibration at millikelvin temperatures," *Rev. Sci. Instrum.*, vol. 84, no. 3, Mar. 2013, Art. no. 034704.
[15] S. Krinner, S. Storz, P. Kurpiers, P. Magnard, J. Heinsoo, R. Keller, J. Lütolf, C. Eichler, and A. Wallraff, "Engineering cryogenic setups for 100-qubit scale superconducting circuit systems," *EPJ Quantum Technol.*, vol. 6, no. 1, May 2019.
[16] T. Walter, P. Kurpiers, S. Gasparinetti, P. Magnard, A. Potočnik, Y. Salathé, M. Pechal, M. Mondal, M. Oppliger, C. Eichler, and A. Wallraff, "Rapid high-fidelity single-shot dispersive readout of superconducting qubits," *Phys. Rev. A, Gen. Phys.*, vol. 7, no. 5, May 2017, Art. no. 054020.
[17] M. D. Hutchings, J. B. Hertzberg, Y. Liu, N. T. Bronn, G. A. Keefe, M. Brink, J. M. Chow, and B. L. T. Plourde, "Tunable superconducting qubits with flux-independent coherence," *Phys. Rev. A, Gen. Phys.*, vol. 8, no. 4, Oct. 2017, Art. no. 044003.
[18] T. Hönigl-Decrinis, R. Shaikhaidarov, S. E. de Graaf, V. N. Antonov, and O. V. Astafiev, "Two-level system as a quantum sensor for absolute calibration of power," *Phys. Rev. A, Gen. Phys.*, vol. 13, no. 2, Feb. 2020, Art. no. 024066.
[19] D. M. Pozar, *Microwave Engineering*. Wiley, 2005, pp. 193–196, ch. 4.
[20] G. F. Engen and C. A. Hoer, "Thru-reflect-line: An improved technique for calibrating the dual six-port automatic network analyzer," *IEEE Trans. Microw. Theory Techn.*, vol. MTT-27, no. 12, pp. 987–993, Dec. 1979.
[21] B. C. Wadell, *Transmission Line Design Handbook*. Norwood, MA, USA: Artech House, 1991, p. 79.
[22] Mini-Circuits. *BW-S10W2+, 10 dB Fixed Attenuator, 50?*. [Online]. Available: https://www.minicircuits.com/WebStore/dashboard.html?model=BW-S10W22B
[23] R. B. Marks, "Formulations of the basic vector network analyzer error model including switch-terms," in *Proc. 50th ARFTG Conf. Dig.*, vol. 32, Dec. 1997, pp. 115–126.
[24] D. F. Williams and R. B. Marks, "Transmission line capacitance measurement," *IEEE Microw. Guided Wave Lett.*, vol. 1, no. 9, pp. 243–245, Sep. 1991.
[25] R. B. Marks and D. F. Williams, "Characteristic impedance determination using propagation constant measurement," *IEEE Microw. Guided Wave Lett.*, vol. 1, no. 6, pp. 141–143, Jun. 1991.
[26] A. Y. Dmitriev, R. Shaikhaidarov, T. Hönigl-Decrinis, S. E. de Graaf, V. N. Antonov, and O. V. Astafiev, "Probing photon statistics of coherent states by continuous wave mixing on a two-level system," *Phys. Rev. A, Gen. Phys.*, vol. 100, no. 1, Jul. 2019, Art. no. 013808.
[27] F. Arute, K. Arya, R. Babbush, D. Bacon, J. C. Bardin, R. Barends, R. Biswas, S. Boixo, F. G. Brandao, D. A. Buell, and B. Burkett, "Quantum supremacy using a programmable superconducting processor," *Nature*, vol. 574, no. 7779, pp. 505–510, Oct. 2019.
[28] X. Xue, B. Patra, J. P. G. van Dijk, N. Samkharadze, S. Subramanian, A. Corna, B. P. Wuetz, C. Jeon, and F. Sheikh, "CMOS-based cryogenic control of silicon quantum circuits," *Nature*, vol. 593, no. 7858, pp. 205–210, May 2021.
[29] C. Yan, J. Hassel, V. Vesterinen, J. Zhang, J. Ikonen, L. Grönberg, J. Goetz, and M. Möttönen, "A low-noise on-chip coherent microwave source," *Nature Electron.*, vol. 4, no. 12, pp. 885–892, Dec. 2021.
[30] D. Zhang and J.-S. Tsai, "Magnetic-free traveling-wave nonreciprocal superconducting microwave components," *Phys. Rev. A, Gen. Phys.*, vol. 15, no. 6, Jun. 2021, Art. no. 064013.
[31] K. M. Sliwa, M. Hatridge, A. Narla, S. Shankar, L. Frunzio, R. J. Schoelkopf, and M. H. Devoret, "Reconfigurable Josephson circulator/directional amplifier," *Phys. Rev. X*, vol. 5, no. 4, Nov. 2015, Art. no. 041020.
[32] M. Pechal, J.-C. Besse, M. Mondal, M. Oppliger, S. Gasparinetti, and A. Wallraff, "Superconducting switch for fast on-chip routing of quantum microwave fields," *Phys. Rev. A, Gen. Phys.*, vol. 6, no. 2, Aug. 2016, Art. no. 024009.
[33] M. Colangelo, D. Zhu, D. F. Santavicca, B. A. Butters, J. C. Bienfang, and K. K. Berggren, "Compact and tunable forward coupler based on high-impedance superconducting nanowires," *Phys. Rev. A, Gen. Phys.*, vol. 15, no. 2, Feb. 2021, Art. no. 024064.
[34] J. Aumentado, "Superconducting parametric amplifiers: The state of the art in Josephson parametric amplifiers," *IEEE Microw. Mag.*, vol. 21, no. 8, pp. 45–59, Aug. 2020.
[35] X. Gu, A. F. Kockum, A. Miranowicz, Y. X. Liu, and F. Nori, "Microwave photonics with superconducting quantum circuits," *Phys. Rep.*, vols. 718–719, pp. 1–102, Nov. 2017.
[36] *Agilent Application Note AN 1287-3*, Agilent Technologies, Santa Clara, CA, USA, 1998.

MANOJ STANLEY (Member, IEEE) received the Ph.D. degree in electrical engineering from the University of Liverpool, in 2019. After the completion of his Ph.D. degree, he joined the National Physical Laboratory, Electromagnetic Technologies Group, U.K., as a Higher Research Scientist. He has supported the development of next-generation computing and communications technologies and high-frequency electronics applications. This includes design and characterization of devices at RF and terahertz frequencies, RF metrology for quantum computing applications, material and channel characterization for 5G, and beyond communication. Currently, he is developing high-frequency metrology capabilities to characterize superconducting quantum integrated circuits at milli-kelvin temperatures. He is the Operations Officer for European Microwave Week 2021.

SEBASTIAN DE GRAAF works with the National Physical Laboratory.

TERESA HÖNIGL-DECRINIS received the Ph.D. degree in physics from Royal Holloway, University of London, in 2018, where she developed a novel quantum technology, the Absolute Power Quantum Sensor, under supervision of Prof. Oleg Astafiev. She subsequently joined the National Physical Laboratory, Quantum Technology Team, as a Higher Research Scientist and a Measurement Fellow to lead efforts in the optimization of this novel quantum technology. She has been recently awarded the Lise Meitner Fellowship from the Austrian Science Fund (FWF) and moved to the Institute for Quantum Optics and Quantum Information (IQOQI), Austrian Academy of Sciences, Innsbruck.

TOBIAS LINDSTRÖM works with the National Physical Laboratory.

NICK M. RIDLER (Fellow, IEEE) received the B.Sc. degree from the King's College London, University of London, London, U.K., in 1981. He is currently the Head of Science with the National Physical Laboratory (NPL), Electromagnetic and Electrochemical Technologies Department, U.K. He is a NPL Fellow and a Honorary Professor with the University of Glasgow and University of Liverpool, U.K., and, a Visiting Professor with the University of Kent, University of Leeds, and University of Surrey, U.K. He is also a Non-Executive Director of LA Techniques Ltd., a fellow of the Institution of Engineering and Technology (IET) and a fellow of the Institute of Physics (IOP). He has more than 35 year's experience working in industrial, government, and academic research establishments. His research interest includes precision high-frequency electromagnetic measurement (from one kHz to one THz).